PHYSICAL REVIEW A **96**, 061601(R) (2017)

Visualizing the BEC-BCS crossover in a two-dimensional Fermi gas: Pairing gaps and dynamical response functions from *ab initio* computations

Ettore Vitali, Hao Shi, Mingpu Qin, and Shiwei Zhang
Department of Physics, College of William and Mary, Williamsburg, Virginia 23187, USA
(Received 23 May 2017; published 4 December 2017)

Experiments with ultracold atoms provide a highly controllable laboratory setting with many unique opportunities for precision exploration of quantum many-body phenomena. The nature of such systems, with strong interaction and quantum entanglement, makes reliable theoretical calculations challenging. Especially difficult are excitation and dynamical properties, which are often the most directly relevant to experiment. We carry out exact numerical calculations, by Monte Carlo sampling of imaginary-time propagation of Slater determinants, to compute the pairing gap in the two-dimensional Fermi gas from first principles. Applying state-of-the-art analytic continuation techniques, we obtain the spectral function and the density and spin structure factors providing unique tools to visualize the BEC-BCS crossover. These quantities will allow for a direct comparison with experiments.

DOI: 10.1103/PhysRevA.96.061601

It is truly unusual when, starting from a microscopic Hamiltonian, theory can achieve an exact description of a strongly correlated fermionic system which, at the same time, can be realized in a laboratory with great precision and control. Experiments with ultracold atoms [1,2] have provided a possibility to realize such a scenario. The accuracy that can be reached in experiments with Fermi atomic gases and optical lattices is exceptional, thus offering a unique setting to explore highly correlated quantum fermion systems. In this Rapid Communication, we demonstrate that, from the theoretical side, advances in computational methods now make it feasible to obtain numerically exact results for not only equilibrium properties but also excited states. We compute the pairing gap, spectral functions, and dynamical response functions in the two-dimensional Fermi gas across the range of interactions, which will allow direct comparisons with spectroscopy or scattering experiments. The dynamical properties provide a powerful tool to probe the behavior of the system and to visualize the crossover from a gas of molecules to a BCS superfluid.

We study the Fermi gas with a zero-range attractive interaction, which has generated a great deal of research activity [1–15]. The interest of the system is very wide, ranging from condensed matter physics [6,16] to nuclear physics, with possible important applications also in the study of neutron stars [17,18]. This system describes experiments with a collection of atoms, for example ^{6}Li, which are cooled to degeneracy in an equal mixture of two hyperfine ground states, labeled $|\uparrow\rangle$ and $|\downarrow\rangle$. Feshbach resonances allow the tuning of the interactions by varying an external magnetic field, making the system a unique laboratory to explore many-body physics [19,20]. Starting from a weakly interacting BCS regime, where the attraction between particles induces a pairing similar to the one observed in ordinary superconductors, a crossover is observed as the interaction strength is increased, leading to a BEC regime where the Cooper pairs are tightly bound such that the system behaves as a gas of bosonic molecules. While both the BCS and the BEC regimes are well understood, the crossover regime provides an excellent example of a strongly interacting quantum many-body system [1,2].

We focus in particular on the two-dimensional (2D) Fermi gas, which has recently been realized experimentally using a highly anisotropic trapping potential [4,5]. The 2D system is important, since some of the most interesting physical phenomena, such as high-temperature superconductivity [21], Dirac fermions in graphene [22] and topological superconductors [23], and nuclear "pasta" phases [24] in neutron stars, are two-dimensional in nature. Quantum fluctuations are known to be enhanced in 2D, making it even more important to have quantitative results beyond mean-field approaches.

Experiments are just beginning to measure properties in the 2D gas [8,11,13,25,26]. An array of calculations [16,27–34] has been performed, including for spectral functions [35–39] (mostly for above the critical temperature). Numerical results free of any uncontrolled approximations would provide an unambiguous benchmark for theory and allow direct comparison with experiments as lower temperatures are reached. As is the case across a variety of systems in condensed matter and cold atoms, dynamical properties and spectral information are crucial, since they provide the most direct connection with experiments. However they are much more challenging to compute than static properties [40].

In this Rapid Communication, we develop the capabilities to obtain unbiased results for imaginary-time correlation functions in spin-balanced Fermi gas systems, using first-principles auxiliary-field quantum Monte Carlo (AFQMC) [41–44] methods. This provides a unique approach to excitations and dynamical response functions. Focusing on the BEC-BCS crossover regime, we compute the pairing gap as a function of the interaction strength, the spectral function, which can be measured experimentally in photoemission spectroscopy [25], and the density and spin structure factors, which can be measured in two-photon scattering experiments [45].

As the range of the interaction in the Fermi gas system of cold atoms is much smaller than the average interparticle distance, the system can be modeled using a lattice Hamiltonian [46]:

$$\hat{H} = t \sum_{\vec{k},\sigma} \varepsilon(\vec{k})\, \hat{c}^{\dagger}_{\vec{k},\sigma} \hat{c}_{\vec{k},\sigma} + U \sum_{i} \hat{n}_{i,\uparrow} \hat{n}_{i,\downarrow}, \qquad (1)$$

where the label i runs over a square lattice with $\mathcal{N}_s = L \times L$ sites hosting a total of $\mathcal{N}_p$ fermions, half with each spin σ ($=\uparrow$ or $\downarrow$). The momentum $\vec{k} = (k_x, k_y)$ is defined on the reciprocal lattice with units $2\pi/L$ and $k_x, k_y \in [-\pi, \pi)$. The dispersion is $\varepsilon(\mathbf{k}) = k_x^2 + k_y^2$ and $t = \hbar^2/(2mb^2)$, with b the lattice parameter. The attractive on-site interaction U/t is tuned [29,46] for each lattice density $n = \mathcal{N}_p/\mathcal{N}_s$ and Fermi momentum $k_F = \sqrt{2\pi n}/b$ to produce the desired scattering length a, defined as the position of the node of the zero-energy s-wave solution of the two-body problem. In the dilute limit, Eq. (1) provides a regularization of the fundamental Hamiltonian of the dilute atomic gas in the continuum. We ensure that proper diluteness conditions are met in the computations, and then apply a careful extrapolation procedure to the continuum limit [29,47].

The ground-state wave function $|\Psi_0\rangle$ of $\hat{H}$ is sampled using the AFQMC method [29]. For Hamiltonian (1) with $U/t < 0$, the sampling is not affected by the sign problem, so that numerical results can be obtained free of any bias for each set of parameters $\{\mathcal{N}_s, \mathcal{N}_p, U/t\}$. Accelerated sampling techniques with force bias are used, together with other technical improvements [48], which greatly improves the efficiency of our calculations.

Our computation here relies on an algorithm which improved the computational scaling in the calculation of imaginary-time correlation functions [49] from $O(\mathcal{N}_s^3)$ in standard algorithms [50–55] to $O(\mathcal{N}_s \mathcal{N}_p^2)$. The algorithm lets fluctuations related to creation and destruction operators or density and spin operators propagate in imaginary time, coupled to the stochastic evolution of the underlying AFQMC random walk or path integral [49]. The dynamical correlation functions are obtained as suitable combinations of matrix elements involving the Slater determinants [49]. In the Fermi gas systems, the calculation is at the dilute limit, with $\mathcal{N}_s \gg \mathcal{N}_p$, so that a drastic speedup is achieved. This allows us to study lattices of $\mathcal{N}_s \sim 2000$ sites in order to, as illustrated below, reach proper convergence of the results to the continuum and then to the thermodynamic limit.

The exact imaginary-time correlation functions allow one to access a number of important physical quantities. We compute the pairing gap Δ from the large imaginary-time behavior of the dynamical Green's functions:

$$G^p(\vec{k},\tau) = \langle\, \hat{c}_{\vec{k}}\, e^{-\tau(\hat{H}-E_0)}\, \hat{c}^\dagger_{\vec{k}} \rangle,$$
$$G^h(\vec{k},\tau) = \langle\, \hat{c}^\dagger_{\vec{k}}\, e^{-\tau(\hat{H}-E_0)}\, \hat{c}_{\vec{k}} \rangle, \qquad (2)$$

where the superscripts p and h indicate particle and hole, and E_0 is the ground-state energy. The usual definition of Δ, involving the ground-state energies for systems with $\mathcal{N}_p \pm 1$ particles,

$$E_0^{\mathcal{N}_p+1} - E_0^{\mathcal{N}_p} = \mu + \Delta, \quad E_0^{\mathcal{N}_p-1} - E_0^{\mathcal{N}_p} = -\mu + \Delta, \quad (3)$$

can be recast in terms of the Green's functions, whose spectral resolution yields the asymptotic behavior:

$$G^p(\vec{k},\tau) \simeq c^p(\vec{k}) e^{-\tau E_+(\vec{k})}, \quad G^h(\vec{k},\tau) \simeq c^h(\vec{k}) e^{-\tau E_-(\vec{k})}. \quad (4)$$

The relations in Eq. (4) define the quasiparticle energies $E_\pm(\vec{k})$, with

$$\Delta = \min_{\vec{k}} [E_+(\vec{k}) - \mu], \qquad (5)$$

and a similar relation for the holes. Since we can compute the chemical potential μ exactly [29], we do not need both particle and hole correlation functions. We checked, however, that the two always give compatible results for the pairing gap. In order to compute the quasiparticle dispersion $E_+(\vec{k})$ from $G^p(\vec{k},\tau)$, we fitted $G^p(\vec{k},\tau)$ with a linear combination of two exponentials on an interval $[\tau_0, \tau_{\max}]$, the lower-energy exponent yielding $E_+(\vec{k})$, while the higher-energy exponential is meant to capture residual effects at finite τ besides the asymptotic behavior of Eq. (4). We estimate the statistical uncertainty on $E_+(\vec{k})$ from a conservative combination of the AFQMC error bars on $G^p(\vec{k},\tau)$, uncertainty on the fitting parameters, and dependence on the choice of the interval $[\tau_0, \tau_{\max}]$, randomly sampling τ_0 in the large imaginary-time tail of $G^p(\vec{k},\tau)$. We scan $\vec{k}$ to locate the minimum and maximum (for the particle and hole Green's functions) or the pairing gap, as shown in Fig. 2.

We comment that the standard approach to determine the pairing gap, via addition or removal energies as defined in Eq. (3), would require separate calculations corresponding to different particle numbers. While the spin-balanced calculation is free of the sign problem, the $(\mathcal{N}_p \pm 1)$ calculations are not. Our approach through imaginary-time Green's functions is advantageous, since the Monte Carlo sampling remains at $\mathcal{N}_p$ and thus sign-problem free [49]. In the Supplemental Material [69] we further illustrate our procedure with figures. A comparison with exact diagonalization is made. We also list the values of the computed $E_\pm(\vec{k})$ in a neighborhood of the minimum, which will provide a valuable benchmark.

We compute the spectral function

$$A(\vec{k},\omega) = \langle\, \hat{c}_{\vec{k}}\, \delta(\omega - \hat{H})\, \hat{c}^\dagger_{\vec{k}} \rangle + \langle \hat{c}^\dagger_{\vec{k}}\, \delta(\omega + \hat{H})\, \hat{c}_{\vec{k}} \,\rangle \qquad (6)$$

and the density and spin dynamical structure factors

$$S^{\hat{O}}(\vec{k},\omega) = \langle\, \hat{O}_{\vec{k}}\, \delta(\omega - \hat{H})\, \hat{O}_{-\vec{k}} \,\rangle, \qquad (7)$$

where the operator $\hat{O}$ is $\rho_{\vec{k}} = \hat{n}_{\vec{k},\uparrow} + \hat{n}_{\vec{k},\downarrow}$ for density and $S_{\vec{k}} = (\hat{n}_{\vec{k},\uparrow} - \hat{n}_{\vec{k},\downarrow})/2$ for spin, and the brackets indicate ground-state expectations. These functions are obtained from analytic continuation of the imaginary-time Green's functions and density-density or spin-spin correlation functions, using the genetic inversion via falsification of theories (GIFT) method [56–62]. It is important to note that while the computations of the imaginary-time correlation functions, the quasiparticle energies, and the pairing gaps are exact, the estimation of the spectral function $A(\vec{k},\omega)$ in the full $(\vec{k},\omega)$ plane and that of the (spin) density dynamical structure factors require analytic continuation, which is ill posed and thus has intrinsic limitations. Our tests indicate that the procedure here with GIFT is quite robust; however there is no exactness property in these quantities.

Figure 1 shows the computed pairing gap across different interaction strengths. We also show the BCS mean-field prediction, as well as the current best many-body results, from recent diffusion Monte Carlo (DMC) calculations [30,31]. It is seen that our pairing gap is compatible with the DMC results on the BEC side of the crossover, but is consistently smaller for larger values of $\ln(k_F a)$. The smaller gap value is not surprising, since the DMC contains a fixed-node (FN)

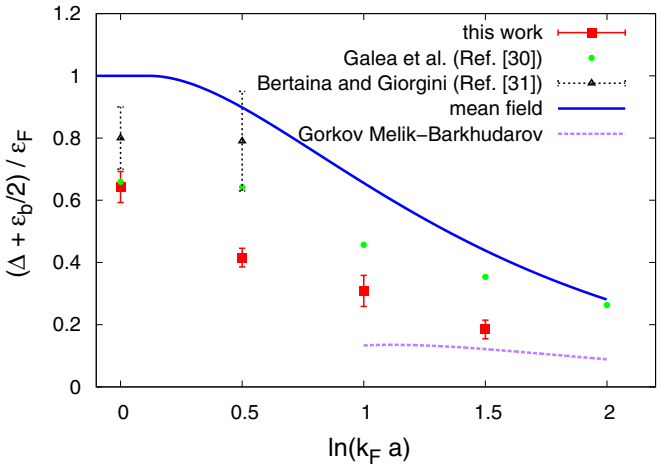

FIG. 1. Pairing gap as a function of interacting strength, $\ln(k_F a)$. The gap values have been shifted by the binding energy, ε_b. DMC results are from Refs. [30] (circles) and [31] (triangles). BCS mean-field result is also shown for reference.

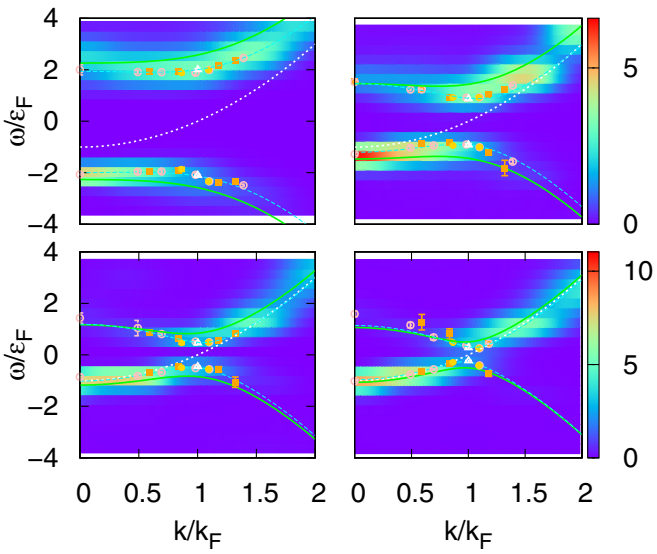

FIG. 2. Computed quasiparticle peaks and spectral functions. The four panels are for different values of the interaction parameter: $\ln(k_F a) = 0$ (top left), $\ln(k_F a) = 0.5$ (top right), $\ln(k_F a) = 1$ (bottom left), $\ln(k_F a) = 1.5$ (bottom right). Energies are measured in units of the Fermi energy $\varepsilon_F = \hbar^2 k_F^2/2m$ and momenta in units of the Fermi momentum k_F. The zero of the energy is set to the chemical potential. The BCS-theory predictions for the quasiparticle energies $E_\pm(\vec{k})$ are shown by solid lines, while the noninteracting spectral function is given by the dotted line. The symbols are the quasiparticle peaks directly computed by AFQMC at the given momentum, for systems of 18 particles on a 25×25 lattice (orange filled squares), 26 particles on a 35×35 lattice (pink empty circles), 42 particles on a 39×39 lattice (gold filled circles), and 50 particles on a 41×41 lattice (empty triangles). Error bars are shown but some are smaller than symbol size. The light dashed lines are interpolations in the neighborhood of the minimum. The color plots give the computed spectral functions, in arbitrary units.

approximation which gives an upper bound on the computed energy. It is reasonable to expect that the trial wave function used for FN is of higher quality for the spin-balanced system compared to that for the $(\mathcal{N}_p \pm 1)$ systems, which would lead to an overestimation of the pairing gap. Our results on the BCS side are consistent with the rescaled BCS results $\Delta_{\rm BCS}/e$ from the theory by Gorkov and Melik-Barkhudarov, which is expected to be exact in the BCS limit $\ln(k_F a) \gg 1$ [63,64].

Figure 2 plots the computed quasiparticle peaks as a function of $k \equiv |\vec{k}|$, together with the spectral function, for four values of the interaction parameter. The zero of the energy is set equal to the chemical potential, which we can compute exactly [29]. We will refer to the function $A(\vec{k},\omega)$ as the particle and hole spectral function respectively for $\omega > \mu$ and $\omega < \mu$. The particle spectral function originates from the first term on the right in Eq. (6), physically representing states available for additional particles injected into the system, while the hole spectral function, originating from the second term, contains information about states occupied by the particles in the system, which are thus accessible by the creation of holes. In each panel, we show also the mean-field prediction for the quasiparticle energies [65]: $E_\pm(\vec{k}) = \pm\sqrt{(\hbar^2k^2/2m - \mu_{\rm BCS})^2 + \Delta_{\rm BCS}^2}$, where $\Delta_{\rm BCS}$ is the gap and $\mu_{\rm BCS}$ the chemical potential in BCS theory. The noninteracting spectral function, $A^0(\vec{k},\omega) = \delta(\omega - (\hbar^2k^2/2m - \varepsilon_F))$, is also shown for reference. In the AFQMC spectral functions obtained from the GIFT analysis, shown in the color plot, quasiparticle peaks are still visible, which are broadened from many-body correlations, resulting in a nonzero imaginary part of the self-energy, and are renormalized with respect to the BCS dispersion relations. The quasiparticle peaks computed directly from AFQMC are shown by symbols. These were obtained following the procedure described above. Results from different system sizes are shown, which indicate convergence to the bulk limit within numerical resolution. (Separate calculations were also carried out to verify that these densities are indistinguishable from the dilute limit [29].)

The behavior of the spectral function provides a clear visualization of the BEC-BCS crossover. In the BEC regime at $\ln(k_F a) = 0$, a large gap, of the order of the energy needed to break a molecule, separates the two branches, which are roughly momentum-independent for $k \leqslant k_F$. A smooth evolution of the spectral function is observed. In the BCS regime at $\ln(k_F a) = 1.5$, it starts to resemble the noninteracting behavior, where a gap is still present at the Fermi momentum, as in conventional superconductors. The intermediate values of the interaction show a smooth crossover between the two regimes. Viewed in the reverse direction, gradual and significant departures from the BCS results are seen as the interaction strength is increased.

We also compute two-body dynamical correlations in imaginary time, which can again be obtained using our method with computational cost linear in $\mathcal{N}_s$ [49]. From these, we apply analytic continuation to obtain the density and spin dynamical structure factors, $S^\rho(\vec{k},\omega)$ and $S^S(\vec{k},\omega)$, which can be measured experimentally using two-photon Bragg spectroscopy [45]. In particular, the high-momentum behavior is very interesting as it provides a highly sensitive probe of the BEC-BCS crossover. We focus our attention on $k = 4k_F$, close to the value recently investigated experimentally in three dimensions [45].

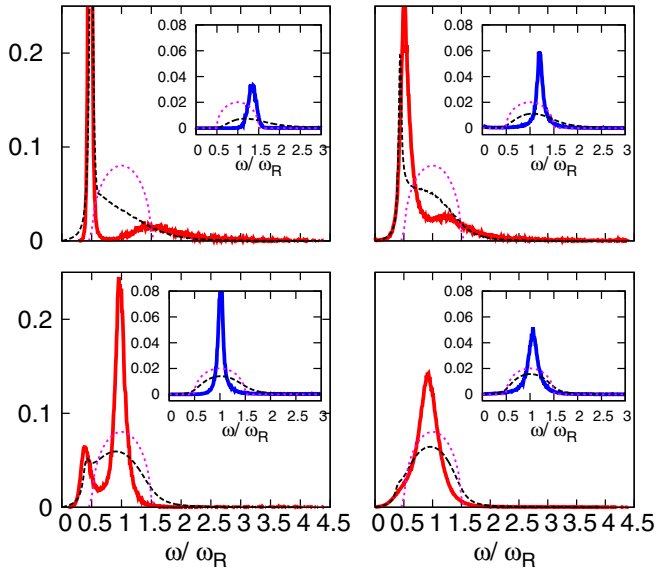

FIG. 3. Density (main graphs) and spin (insets) dynamical structure factors, in units of ε_F^{-1}, at $k = 4k_F$. The four panels show four different values of the interaction parameter: $\ln(k_F a) = 0$ (top left), $\ln(k_F a) = 0.5$ (top right), $\ln(k_F a) = 1$ (bottom left), $\ln(k_F a) = 1.5$ (bottom right). Solid red lines are AFQMC results, while dashed black lines are obtained from dynamical BCS theory. The noninteracting results are also shown (dotted magenta line) in each for reference. The energies on the horizontal axes are measured in units of the atomic recoil energy, $\omega_R = \hbar^2 k^2/2m$.

The results are plotted in Fig. 3 as functions of the frequency ω for the four values of the interaction parameter. In addition to AFQMC, we have also performed self-consistent dynamical BCS theory calculations for the same system, following the approach in Ref. [66] which studied the three-dimensional Fermi gas. The results are shown in the figure for comparison. Because the theory yields the response functions directly, it helps to provide an additional gauge on the reliability of analytic continuation analysis. We observe that the dynamical BCS theory gives results on the response functions that are qualitatively reasonable. Significant differences arise from the AFQMC results, however, for example in the peak position in the spin structure factor for strong interactions. Direct comparisons of the imaginary-time correlation functions show significant differences between AFQMC and dynamical BCS theory as well [47], manifesting particle correlation effects absent in the latter.

In the density response, a large peak is seen at $\omega \simeq \omega_R/2$ in the deep BEC regime. Since the particles are tightly paired to form molecules in this regime, the response of the system at high momentum is dominated by the recoil of the molecules themselves, whose mass is twice the atomic mass. In contrast, the response on the BCS side is simply a free-particle recoil with the bare mass of the atoms. The behavior of the density response in the crossover regime interpolates between the two physical pictures, as is evident from Fig. 3. Starting from $\ln(k_F a) = 0$, we observe a gradual shift of the spectral weight from the dominant molecular contribution towards the second peak at $\omega \simeq \omega_R$. At $\ln(k_F a) = 1$, the second peak dominates, and the molecule peak almost disappears. By $\ln(k_F a) = 1.5$, the response becomes qualitatively similar to the noninteracting one.

The spin response, on the other hand, is not sensitive to the molecular mode at $\omega \simeq \omega_R/2$, since the positive and negative fluctuations on the spin-↑ and spin-↓ particles cancel each other. However, we observe that, as it happens in three-dimensions [45], the intensity of the peak is smaller on the BEC side of the crossover, and the position of the peak is shifted towards higher energies. This corresponds to a suppression of the spin susceptibility, related to the increased energy required to remove atoms from the molecules.

In summary, we have performed *ab initio* calculations of the pairing gaps and dynamical correlation functions for the two-dimensional interacting Fermi atomic gas. Numerically exact AFQMC predictions are provided for the pairing gap. From unbiased imaginary-time correlation functions computed by AFQMC for the many-body ground state, the spectral function and the density and spin dynamical structure factors are obtained, via analytic continuation, across the BEC-BCS crossover. Much larger system sizes are reached in our simulations by the development and implementation of several technical advances. Many internal validations and self-consistency checks are performed and careful error quantifications are carried out to maximize the robustness and reliability of the results. The results will allow benchmarks of further theoretical and computational developments, and direct comparisons with experiments. The exact pairing gaps will also be crucial as an input for formulating a functional in 2D for density-functional theory calculations [67,68]. Excitations and dynamical correlation functions provide excellent tools for visualizing the BEC-BCS crossover. In interacting many-fermion systems in general, they connect directly with experimentally accessible measurements. Our approach opens up many new possibilities for the computational studies of strongly interacting fermionic cold-atomic systems. It is hoped that the results presented here will also serve as an illustration of state-of-the-art computational capabilities, and will stimulate additional theoretical and experimental activities. The feedback from such activities will in turn spur further computations and additional developments.

We thank J. Carlson, A. Gezerlis, and Lianyi He for helpful discussions. This work was supported by NSF (Grant No. DMR-1409510). E.V. and S.Z. were also supported by the Simons Foundation. Computing was carried out at the Extreme Science and Engineering Discovery Environment (XSEDE), which is supported by National Science Foundation Grant No. ACI-1053575, and the computational facilities at William and Mary.

[1] I. Bloch, J. Dalibard, and W. Zwerger, Rev. Mod. Phys. **80**, 885 (2008).

[2] S. Giorgini, L. P. Pitaevskii, and S. Stringari, Rev. Mod. Phys. **80**, 1215 (2008).

[3] J. Carlson, S.-Y. Chang, V. R. Pandharipande, and K. E. Schmidt, Phys. Rev. Lett. **91**, 050401 (2003).
[4] K. Martiyanov, V. Makhalov, and A. Turlapov, Phys. Rev. Lett. **105**, 030404 (2010).
[5] B. Fröhlich, M. Feld, E. Vogt, M. Koschorreck, W. Zwerger, and M. Köhl, Phys. Rev. Lett. **106**, 105301 (2011).
[6] P. Magierski, G. Wlazłowski, and A. Bulgac, Phys. Rev. Lett. **107**, 145304 (2011).
[7] G. Wlazłowski, P. Magierski, and J. E. Drut, Phys. Rev. Lett. **109**, 020406 (2012).
[8] V. Makhalov, K. Martiyanov, and A. Turlapov, Phys. Rev. Lett. **112**, 045301 (2014).
[9] W. Ong, C. Cheng, I. Arakelyan, and J. E. Thomas, Phys. Rev. Lett. **114**, 110403 (2015).
[10] P. A. Murthy, I. Boettcher, L. Bayha, M. Holzmann, D. Kedar, M. Neidig, M. G. Ries, A. N. Wenz, G. Zürn, and S. Jochim, Phys. Rev. Lett. **115**, 010401 (2015).
[11] M. G. Ries, A. N. Wenz, G. Zürn, L. Bayha, I. Boettcher, D. Kedar, P. A. Murthy, M. Neidig, T. Lompe, and S. Jochim, Phys. Rev. Lett. **114**, 230401 (2015).
[12] K. Fenech, P. Dyke, T. Peppler, M. G. Lingham, S. Hoinka, H. Hu, and C. J. Vale, Phys. Rev. Lett. **116**, 045302 (2016).
[13] I. Boettcher, L. Bayha, D. Kedar, P. A. Murthy, M. Neidig, M. G. Ries, A. N. Wenz, G. Zürn, S. Jochim, and T. Enss, Phys. Rev. Lett. **116**, 045303 (2016).
[14] J. Carlson and S. Reddy, Phys. Rev. Lett. **95**, 060401 (2005).
[15] Z. Luo, C. E. Berger, and J. E. Drut, Phys. Rev. A **93**, 033604 (2016).
[16] M. Bauer, M. M. Parish, and T. Enss, Phys. Rev. Lett. **112**, 135302 (2014).
[17] A. Gezerlis and J. Carlson, Phys. Rev. C **77**, 032801 (2008).
[18] D. Lacroix, Phys. Rev. A **94**, 043614 (2016).
[19] C. Chin, R. Grimm, P. Julienne, and E. Tiesinga, Rev. Mod. Phys. **82**, 1225 (2010).
[20] I. Bloch, J. Dalibard, and S. Nascimbene, Nat. Phys. **8**, 267 (2012).
[21] P. A. Lee, N. Nagaosa, and X.-G. Wen, Rev. Mod. Phys. **78**, 17 (2006).
[22] A. H. Castro Neto, F. Guinea, N. M. R. Peres, K. S. Novoselov, and A. K. Geim, Rev. Mod. Phys. **81**, 109 (2009).
[23] X.-L. Qi and S.-C. Zhang, Rev. Mod. Phys. **83**, 1057 (2011).
[24] Y. Yu and A. Bulgac, Phys. Rev. Lett. **90**, 161101 (2003).
[25] M. Feld, B. Frohlich, E. Vogt, M. Koschorreck, and M. Kohl, Nature (London) **480**, 75 (2011).
[26] C. Cheng, J. Kangara, I. Arakelyan, and J. E. Thomas, Phys. Rev. A **94**, 031606 (2016).
[27] L. He, H. Lü, G. Cao, H. Hu, and X.-J. Liu, Phys. Rev. A **92**, 023620 (2015).
[28] M. Klawunn, Phys. Lett. A **380**, 2650 (2016).
[29] H. Shi, S. Chiesa, and S. Zhang, Phys. Rev. A **92**, 033603 (2015).
[30] A. Galea, H. Dawkins, S. Gandolfi, and A. Gezerlis, Phys. Rev. A **93**, 023602 (2016).
[31] G. Bertaina and S. Giorgini, Phys. Rev. Lett. **106**, 110403 (2011).
[32] E. R. Anderson and J. E. Drut, Phys. Rev. Lett. **115**, 115301 (2015).
[33] L. Rammelmüller, W. J. Porter, and J. E. Drut, Phys. Rev. A **93**, 033639 (2016).
[34] M. Matsumoto, D. Inotani, and Y. Ohashi, Phys. Rev. A **93**, 013619 (2016).
[35] F. Marsiglio, P. Pieri, A. Perali, F. Palestini, and G. C. Strinati, Phys. Rev. B **91**, 054509 (2015).
[36] A. Perali, F. Palestini, P. Pieri, G. C. Strinati, J. T. Stewart, J. P. Gaebler, T. E. Drake, and D. S. Jin, Phys. Rev. Lett. **106**, 060402 (2011).
[37] R. Watanabe, S. Tsuchiya, and Y. Ohashi, Phys. Rev. A **88**, 013637 (2013).
[38] M. Barth and J. Hofmann, Phys. Rev. A **89**, 013614 (2014).
[39] B. C. Mulkerin, K. Fenech, P. Dyke, C. J. Vale, X.-J. Liu, and H. Hu, Phys. Rev. A **92**, 063636 (2015).
[40] L. He, Ann. Phys. (NY) **373**, 470 (2016).
[41] S. Zhang, in *Auxiliary-Field Quantum Monte Carlo for Correlated Electron Systems*, edited by E. Pavarini, E. Koch, and U. Schollwöck, Vol. 3 of Emergent Phenomena in Correlated Matter: Modeling and Simulation (Verlag des Forschungszentrum Jülich, Jülich, 2013).
[42] J. P. F. LeBlanc, A. E. Antipov, F. Becca, I. W. Bulik, G. K.-L. Chan, C.-M. Chung, Y. Deng, M. Ferrero, T. M. Henderson, C. A. Jiménez-Hoyos, E. Kozik, X.-W. Liu, A. J. Millis, N. V. Prokof'ev, M. Qin, G. E. Scuseria, H. Shi, B. V. Svistunov, L. F. Tocchio, I. S. Tupitsyn, S. R. White, S. Zhang, B.-X. Zheng, Z. Zhu, and E. Gull (Simons Collaboration on the Many-Electron Problem), Phys. Rev. X **5**, 041041 (2015).
[43] M. Qin, H. Shi, and S. Zhang, Phys. Rev. B **94**, 085103 (2016).
[44] H. Shi and S. Zhang, Phys. Rev. B **88**, 125132 (2013).
[45] S. Hoinka, M. Lingham, M. Delehaye, and C. J. Vale, Phys. Rev. Lett. **109**, 050403 (2012).
[46] F. Werner and Y. Castin, Phys. Rev. A **86**, 013626 (2012).
[47] E. Vitali, H. Shi, M. Qin, and S. Zhang, J. Low Temp. Phys. **189**, 312 (2017).
[48] H. Shi and S. Zhang, Phys. Rev. E **93**, 033303 (2016).
[49] E. Vitali, H. Shi, M. Qin, and S. Zhang, Phys. Rev. B **94**, 085140 (2016).
[50] J. E. Hirsch, Phys. Rev. B **31**, 4403 (1985).
[51] M. Feldbacher and F. F. Assaad, Phys. Rev. B **63**, 073105 (2001).
[52] F. F. Assaad and M. Imada, Phys. Rev. Lett. **76**, 3176 (1996).
[53] M. Motta, D. E. Galli, S. Moroni, and E. Vitali, J. Chem. Phys. **140**, 024107 (2014).
[54] M. Motta, D. E. Galli, S. Moroni, and E. Vitali, J. Chem. Phys. **143**, 164108 (2015).
[55] Y. Alhassid, M. Bonett-Matiz, S. Liu, A. Mukherjee, and H. Nakada, EPJ Web Conf. **69**, 00010 (2014).
[56] E. Vitali, M. Rossi, L. Reatto, and D. E. Galli, Phys. Rev. B **82**, 174510 (2010).
[57] G. Bertaina, D. E. Galli, and E. Vitali, Adv. Phys.: X **2**, 302 (2017).
[58] G. Bertaina, M. Motta, M. Rossi, E. Vitali, and D. E. Galli, Phys. Rev. Lett. **116**, 135302 (2016).
[59] M. Motta, E. Vitali, M. Rossi, D. E. Galli, and G. Bertaina, Phys. Rev. A **94**, 043627 (2016).
[60] F. Arrigoni, E. Vitali, D. E. Galli, and L. Reatto, Low Temp. Phys. **39**, 793 (2013).
[61] M. Nava, D. E. Galli, S. Moroni, and E. Vitali, Phys. Rev. B **87**, 144506 (2013).
[62] S. Saccani, S. Moroni, and M. Boninsegni, Phys. Rev. Lett. **108**, 175301 (2012).
[63] D. S. Petrov, M. A. Baranov, and G. V. Shlyapnikov, Phys. Rev. A **67**, 031601 (2003).
[64] L. P. Gorkov and T. K. Melik-Barkhudarov, Sov. Phys. JETP **13**, 1018 (1961).

[65] M. Randeria, J.-M. Duan, and L.-Y. Shieh, Phys. Rev. Lett. **62**, 981 (1989).

[66] R. Combescot, M. Y. Kagan, and S. Stringari, Phys. Rev. A **74**, 042717 (2006).

[67] A. Bulgac, Annu. Rev. Nucl. Part. Sci. **63**, 97 (2013).

[68] P. Zou, F. Dalfovo, R. Sharma, X.-J. Liu, and H. Hu, New J. Phys. **18**, 113044 (2016).

[69] See Supplemental Material at http://link.aps.org/supplemental/10.1103/PhysRevA.96.061601 for more information on our procedure for computing the quasi-particle energies and for additional data.